2012 IEEE/RSJ International Conference on
Intelligent Robots and Systems
October 7-12, 2012. Vilamoura, Algarve, Portugal

A Flapping-Wing Micro Air Vehicle with Interchangeable Parts for System Integration Studies

Ranjana Sahai, Kevin C. Galloway, Michael Karpelson, and Robert J. Wood

Abstract— **This paper describes the development of a unique flapping-wing micro air vehicle (FWMAV) whose major components, i.e. the motor, transmission mechanisms, and wings, are rapidly interchangeable. When coupled with a test stand that includes a 6-axis force sensor, encoder, power-recording capabilities, and high speed video, the result is a highly versatile experimental platform on which system integration studies can be conducted. This paper provides a detailed description of the design and fabrication of this FWMAV whose interchangeability of parts is mostly accomplished through a novel system of tabs, slots, and retaining rods. Results of a study on energy saving elements in the transmission mechanism as well as an exploration of this effect for different wing sizes are also presented. Finally, the implications of interchangeable parts on the creation of customizable flyers are discussed.**

I. INTRODUCTION

Advancements in flapping-wing micro air vehicles (FWMAVs) and MAV-related technologies [1], [2], [3] have made the design and fabrication of successful insect or bird-like flyers more feasible for both researchers and hobbyists alike. The design of such FWMAVs typically involves the consideration of three major components: (1) actuator selection and sizing, (2) transmission mechanism selection and design (for converting the actuator motion into flapping motion), and (3) the shape and structure of the wing. In the choice of the actuator, the size and weight of the required circuitry and power source should also be taken into account. Also, although theoretically possible to accomplish with the wings alone, depending on the complexity (i.e., degrees of freedom) of the wing hinge, additional control surfaces might be necessary for stabilization and steering. Indeed, the development of most of the successful flapping flyers at this size involves the consideration of the individual evolution of many of these components [3], [4], [5].

Nevertheless, the typical methodology to optimize the performance of one of these individual elements (i.e., the actuator, transmission, or wing) generally involves the characterization of the element in isolation. For instance, previous tests for determining the effects of wing flexibility on lift, thrust, and power involved testing the wings alone on an individualized setup before their integration into a fully developed prototype [6], [7]. Certain advantages can be gained from an isolated performance study, and indeed limited access or visibility when fully integrated into the system might necessitate isolation of the component. However, many arguments can also be made for conducting tests in a fully integrated system. Such a test would allow all the components to experience the true loading (or a close proximity) that occurs when the entire system functions in unison. In their development of an approximately 19g hummingbird-sized FWMAV at Aerovironment, Keennon, et al. [3] also pointed out the importance of integrated system testing. They noted that a computational approach to optimizing the wing alone can result in a wing with high aerodynamic efficiency but not necessarily in a total system with high propulsive efficiency [3]. Since flapping can result in losses all along the power drive train of the mechanism, it is important to do wing optimization with the entire system taken into account.

In the present work we have taken the integrated approach to collecting such data specifically for FWMAVs in the 2-15 g weight range while still early in the development (prior to flight testing). To accommodate all these studies on a single platform, we have developed a FWMAV testing platform that allows for an easy interchange of parts. The actuator type is limited to DC motors but virtually all of the successful flyers in this weight range use this kind of actuator (see Table 1). The vehicle is coupled to a 6-axis force sensor for measuring forces and torques generated while flapping, an encoder for measuring motor rotation and hence also the flapping frequency, and a simple circuit to record the motor voltage and current. The addition of high-speed cameras to visually record the flapping motion should allow this platform to be useful for a host of studies including wing construction, size, shape, and motion and the addition of elastic storage elements in the transmission design. Furthermore, with some alterations to the body and transmission to make it flight-worthy, adding an on-board power source and electronics, yet retaining the capability of interchanging parts, we hope to develop unique customizable FWMAVs. These FWMAVs should allow their user to select a combination of parts to give the flyer optimal performance for a given mission.

In what follows, we discuss the design of the platform in detail, show results of initial system tests and discuss these results particularly as they apply to the development of future customizable flapping FWMAVs.

II. OVERALL SYSTEM DESIGN

Fig. 1 shows the complete overview of the FWMAV platform with all its interchangeable parts. The main feature that allows the easy interchange is tab and slot mating

This work was partially supported by the Air Force Office of Scientific Research (award #FA9550-10-C-0044) under a subcontract from Physical Sciences Inc. and the Wyss Institute for Biologically Inspired Engineering.

R. Sahai, K. C. Galloway, M. Karpelson, and R. J. Wood are with with the Harvard Microrobotics Laboratory, Harvard University, Cambridge, MA, 02138 USA, and also with the Wyss Institute for Biologically Inspired Engineering, Harvard University, Boston, MA 02115 USA. rsahai@seas.harvard.edu

between parts. The parts are then held securely in place by rods threaded through holes in the tabs. All three of the major components, (1) the motor housing and body, (2) the transmission mechanisms, and (3) the wings, employ this mating strategy, and, thus, each of them have at least some degree of interchangeability. More design and fabrication details of each subsystem and their corresponding degree of interchangeability are provided below.

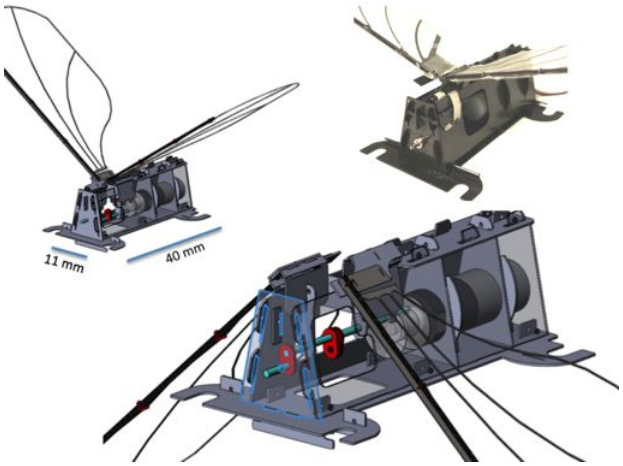

Fig. 1. Both the CAD model and real FWMAV system (top right) and a closeup of the CAD model showing a cutaway of the inside main drivetrain.

A. Motor Housing and Body Design

The motor housing consists of two panels (marked A in Fig. 2) that slide over the front and back of the motor. These two panels are then hooked in place by the two side body panels (B). This whole setup is then placed in a series of small slots in the bottom panel (C), and the assembly is held in place by the insertion of three carbon fiber rods. Two panels for the top (D) and front (E) are similarly attached (again see Fig. 2). All the panels are fabricated by laser micromaching pre-cured carbon fiber layups (see the bottom of Fig. 2). With this design, the motor can be interchanged with any 6mm-diameter motor with an integrated gear head. The motor used in this work is the GM15 25:1 6mm Planetary Gear Pager Motor sold by Solarbotics. By simply cutting a different hole in the panels that house the motor (panels A), the system can be made to accommodate other diameter motors with integrated gear heads.

Future iterations of the design might also consider a system that will allow the use of motors with external gears. The motor is mated to the transmission through a cap (labeled motor cap in Fig. 2) that fits over the shaft. The other side has two holes to mate with the drive shaft that defines the outer crank pin joint and crank-to-coupler pin joint in the four-bar transmission mechanism described in the next section. The U-shaped hooks on the front and back of the bottom panel allow it to be attached to the force sensor in the complete experimental setup described in Section III.

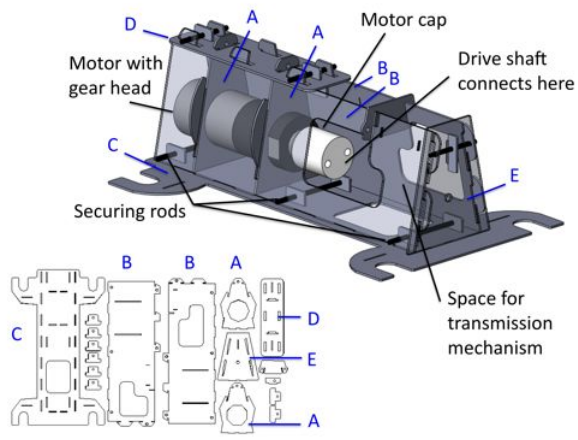

Fig. 2. The CAD model is shown on top. The motor can be interchanged for any 6mm-diameter motor with an integrated gear head. However, a simple modification of the thru hole in the "A" panels (see the bottom cut-file drawing) would allow the use of different sized diameter motors with integrated gear heads.

B. Transmission Mechanisms

Table I presents an overview of some groups that have reported successful lift-off of flapping mechanisms with wing spans of 36 cm or below and weights of 15 g or less. As shown, a common choice for the transmission of a motor-driven flapping mechanism is the four bar and, in particular, the form known as the crank-rocker mechanism. This kind of the four bar consists of a fixed ground link, a crank (which rotates 360 degrees), a coupler link, and a rocker. It provides a natural way to transform the 360 degree rotation of the motor shaft (which drives the crank) to a flapping motion (by connecting the wing to the rocker).

Because of its prevalence, we developed the system here with crank-rocker transmission mechanisms. However, the system can be adapted to use any form of transmission mechanisms as long as it can fit in the space in front of the motor (see Fig. 2).

1) Four-bar Design: The four-bar link lengths should be chosen so that the mechanism operates smoothly and without singularities. A necessary condition for the crank-rocker operation is the Grashof's criterion; that is, the sum of the shortest (the shortest link has to be either crank or the ground) and the longest links be less than the sum of the lengths of the other two links. In addition, the flapping wing attached to the rocker should flap through as large a flap angle (also called the stroke angle) as possible, and the flapping motion should be close to harmonic (sinusoidal). In our present design, we specified a maximum stroke angle of 90 degrees and arbitrarily chose a rocker length of 2 mm. We then determined the length of the other links to achieve this desired flapping operation.

The top left of Fig. 3 shows the two extreme positions of the rocker, $CB1$ and $CB2$ with the included stroke angle ψ_{max}. CD is the bisector of ψ_{max}. By defining the difference between the coupler length $R3$ and the crank length $R2$ as x, it is possible to determine the lengths of the

TABLE I
SMALL FWMAVS WITH SUCCESSFUL LIFT-OFF

Group	Actuator	Transmission	Wingspan	Weight
Harvard Microrobotic Fly [4]	PZT	slider crank to slider crank	3 cm	0.06 g
Clapping wing [8]	Motor	four bar/common crank	10 cm	2.3 g
Micro Delfly [5]	Motor	four bar/equal cranks	10 cm	3.0 g
U Delaware's flyer [9]	Motor	four bar/common crank	36 cm	15.0 g
U Tokyo's flyer [10]	Motor	four bar/common crank	25 cm	6.8 g
U Maryland's flyer [11]	Motor	common crank/ compliant frame	33 cm	12.8 g
Microbat MEMS wing [7]	Motor	four bar/common crank	15 cm	10.5 g

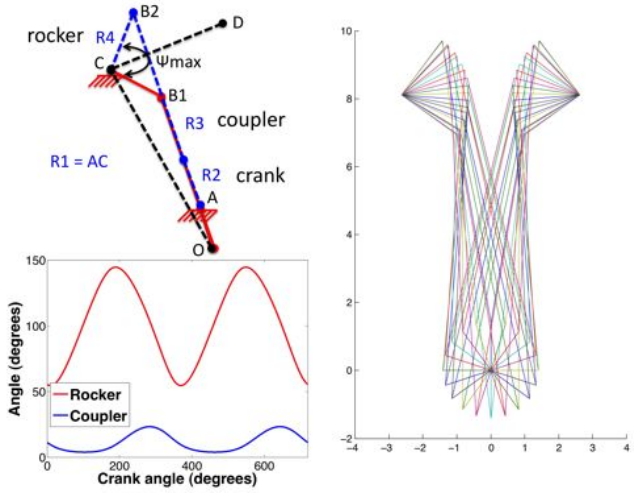

Fig. 3. The top left figure shows how the FWMAV's four-bar transmission link lengths can be designed. In the bottom left figure, the resulting motion of the rocker and coupler is shown as the crank moves through two 360-degree cycles. The right figure shows the simulation of both four-bar transmissions used to determine the phase shift that allows for synchronized flapping.

ground link, crank, and the coupler in terms of x, $R4$, and ψ_{max}. By varying x, and using the resulting link lengths to compute the flapping motion, we determined the combination of link lengths that produces near sinusoidal flapping as shown in the bottom left of Fig. 3. The resulting link lengths are as follows: 1.41 mm crank, 8.41 mm coupler, 2.0 mm rocker, and 8.53 mm ground.

The MATLAB program developed to compute the position, velocity and acceleration during flapping first checks to make sure the mechanism meets the Grashof's criterion. The code then uses the well-known triangular relations and cosine formulas for four-bar linkages to determine the initial configuration of the mechanism in terms of the chosen link lengths. The same procedure is used for incrementally changing the crank position to determine the position configuration as a function of time. An animation of motion is carried out to make sure that the mechanism will operate smoothly and determine any needed phase shift between the two four-bar mechanisms (one for each wing) so that both sides flap in unison as shown in the right of Fig. 3. A Newton Raphson method then determines the corresponding velocities and accelerations.

2) Four-bar and Drive Shaft Fabrication: Because the crank goes through a 360-deg motion, the first two joints of the four-bar mechanism are pin joints. The first joint is simply tied to the motor shaft motion and the second joint is the bottom of the link that is joined to the drive shaft (shown in Fig. 4). The drive shaft is essentially a long pin inserted in the motor cap that defines the outer pin joint of the crank arm. It is a long pin to accommodate the fact that the right four bar must be driven out of phase with respect to the left four bar to produce symmetric flapping. Hence the outer crank pin joint should be slightly shifted from the left outer crank pin joint. The required phase shift is calculated as described earlier or determined from a CAD model. The drive shaft is manufactured with this phase shift (see the bottom of Fig. 4) and is fabricated by holding dowel pins and links in position with the help of the pictured carbon fiber panel jig and then laser welded together. The links in this case are what accomplish the needed bends for the phase shift.

However, since the output link is a rocker and its joints only go through a limited range of motion, these joints can be flexure joints rather than pin joints. Flexure joints were used in our design because of their inherent advantages such as significant weight savings, lower cost and space requirements, as well as reduced wear and lubrication requirements. In addition, the use of flexure joints permits studies in the integration of elastic elements as energy storage elements for the purpose of reducing overall power requirements. Such tests for determining the appropriate elastic spring stiffness in the flexure joints for a given wing have already been carried out [12]. To permit the top two joints to be flexure joints while leaving the bottom two pin joints requires splitting the coupler link into two parts. The top part of the four-bar mechanism is fabricated with flexure joints as shown in the top left of Fig. 4 and described in detail in [12]. The top of the four bar is assembled with the elastic elements (if desired), and then the wing mount is attached. Then the upper half is mated with the lower half as shown in the middle left of Fig. 4. With both four bars assembled on the drive shaft, the drive shaft is then inserted in the motor cap and the opposite sides of the four bars are attached to the body side panels with the same tab, slot and securing rod method as described above, thus, again allowing easy interchange of this top part.

3) Addition of Wing Mounts: The top of the four-bar mechanism (top of Fig. 4) has a tab that interfaces with a wing mount which, in turn, interfaces with the wing. If no elastic elements are being used, then the wing mount can be simply slid on. Otherwise, it has holes which allow the

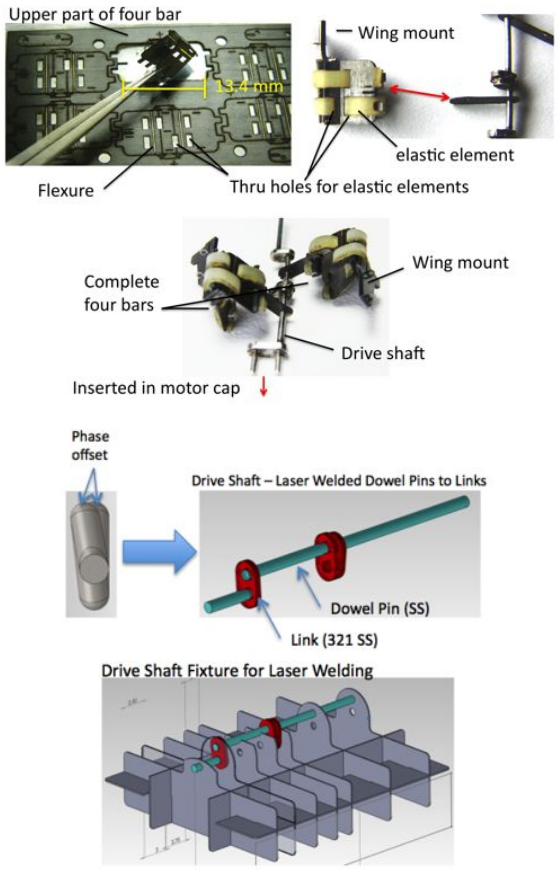

Fig. 4. The top shows the fabrication and assembly of the four bars. The full assembly of both four bars is shown in the middle. The bottom shows the parts of the fabricated drive shaft and the rig used to hold it during laser welding.

elastic elements from the four bar to be threaded over it. The wing mount serves two purposes: (1) as an interface to attach different kinds of wings and (2) to shift the base of the four-bar rockers on both sides so the wing roots line up. Additionally, the wing mounts are separate parts and can be customized, for instance, to allow for a passive rotation joint. In this way, studies similar to the ones conducted on the optimal elastic spring stiffness in the four-bar flexure joints as described in [12] can be carried out on a wing passive rotation joint. Such tests will be conducted on our system in the near future.

C. Interchangeable Wings

The wings mate with the wing mounts attached to the four-bar transmission again through the use of two tabs and a removable carbon fiber rod as shown in blown-up view on the right of Fig. 5. Hence, any wing with this compatible wing root can be mounted and tested on the system. This enables studies of different wing sizes, shapes, and even different material constructions as long as the wing root has two slots of the appropriate size and spacing to slip over the corresponding tabs on the wing mounts.

In the data presented in this paper, we look at variations due to a change in wing size where the aspect ratio remains approximately the same. We also keep the wing fabrication process constant, which consists of cutting the frame and wing spars out of approximately 400 μm thick titanium shim (this material is also used for many of the tabs with holes) with a UV DPSS laser. The resulting frame (as shown in Fig. 5) is then sandwiched between two sheets of 1.5 μm ultra polyester film and pressed together at 215 deg C under a force of approximately 3.5 kN. The leading edge of the wing has several slots. Tabs are inserted in these slots and a carbon fiber rod is threaded through the holes to provide reinforcement to the leading edge.

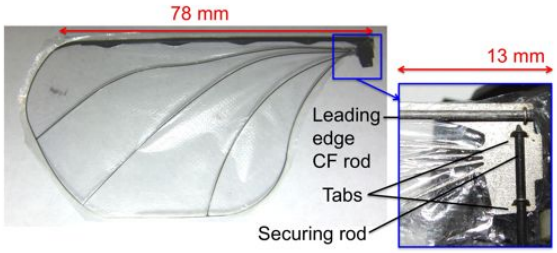

Wing	Area (mm^2)	Inertia about flapping axis ($g\ mm^2$)	Mass (mg)
Small wing	1343	53.3	65
Large wing	2271	141.0	110

Fig. 5. The wing and a blown-up view of a mounted wing root showing the details of the interfacing with the wing mount. The table at the bottom lists the main properties of two different sized wings under consideration.

III. EXPERIMENTAL SETUP

To complete this experimental platform, we interface the FWMAV with several sensors. The full experimental test configuration is shown in Fig. 6. The body of the FWMAV is secured to a six axis force sensor (Nano17, ATI Industrial Automation) via four screws such that the thrust vector of the FWMAV is parallel to the x-axis of the force sensor. The motor driveshaft is extended outside the front of the body and a magnetic encoder (MAE3, US Digital) is attached to record motor rotation speed. In addition to the forces and speed, we also record the voltage and current being supplied to the motor through the use of a simple circuit. The data are recorded via a data acquisition board (NI PCI-6259, National Instruments) and a LabVIEW (National Instruments) program. High speed video is captured with a Casio EX-ZR100 positioned either from the back or from the side while recording at 420 frames per second. Stills captured from a back view recording are shown in Fig. 7.

IV. RESULTS AND DISSCUSSION

A. System Integration Studies

As mentioned in Section II-B.2, this testing system has already been used to carry out a study to determine appropriate spring stiffnesses for latex rubber elements integrated in the top two four-bar flexure joints as energy storage elements.

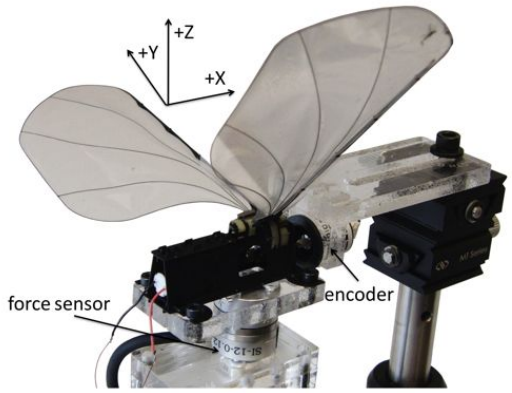

Fig. 6. The complete experimental test setup is shown with the exception of the high speed camera.

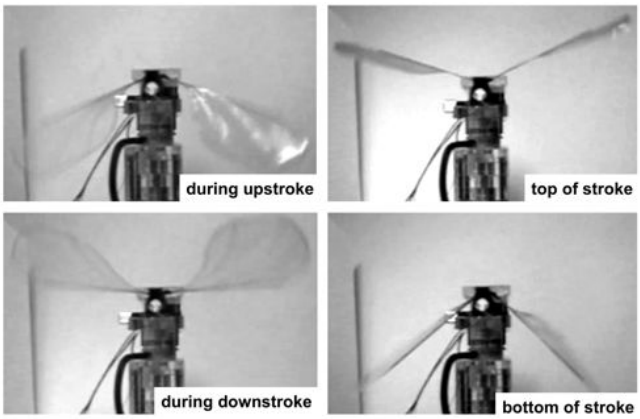

Fig. 7. Stills taken from high speed video capturing the flapping motion during the tests are shown.

While the details can be found in [12], for the particular wing size used in that study (78 mm wing length), the stiffness in the flexure joints (obtained by using 1.02 mm thick latex rubber strips compared to no rubber strips in the flexure joints) produces similar thrust for around 20% less power. Similarly, when operating in the same power region (around 1 W), the 1.02 mm thick flexure case produces around 15-20% more thrust than the no rubber flexure case. This approximately 0.3 g added thrust was achieved with only a 0.02 g cost in weight.

Here we conduct similar tests but with the purpose of seeing the effect of a smaller sized wing (wing length 61 mm). The table in Fig. 5 lists the properties of the two different wings. Using the theoretical motivation developed in [12], we expect an appropriate spring stiffness using thinner latex rubber strips than for the larger wing case (e.g., 0.508 mm thick). At least 5-10 s of flapping were collected and averaged at 11 different voltage settings from 2-6 V. The results of this 0.508 mm stiffness case versus the no rubber case are shown in Fig. 8 along with the two similar cases from the larger wing done in the previous study. We are evaluating the performance based on thrust versus power since it is the most relevant metric for battery-powered flight as considered below. As can be seen in the plot, a similar trend was realized as that in our previously conducted study where the optimal stiffness produces greater thrust compared to the no rubber case for similar power. Since according to classical Rankine Froude theory, we expect the thrust to vary as input power raised to the 2/3 power, a power fit is applied in the figure. The adjusted R-squared values for the fits are 0.9596 and 0.9838 for the large wing, no rubber and 1.02 mm cases, and 0.7930 and 0.8076 for the small wing, no rubber and 0.508 mm cases. The lower quality fits for the small wing are in part due to the fact that fewer trials were conducted here (two) than in the previous study (four).

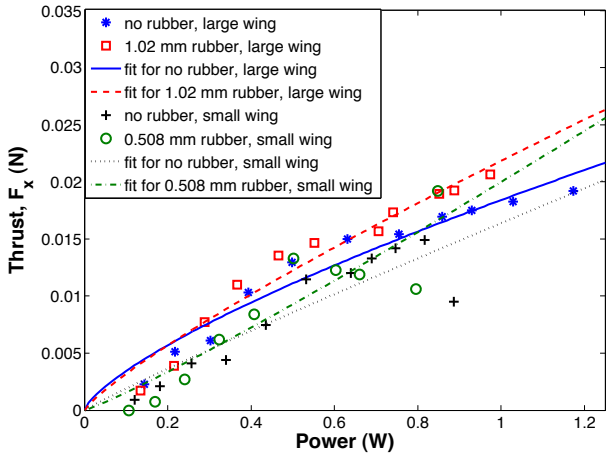

Fig. 8. The results of the experimentally measured thrust versus power are shown for different transmission spring stiffness cases for two different wing sizes.

Also, as expected, the smaller wing results in a smaller power draw compared to the larger size wing and this fact has important implications when we consider the development of customizable flyers as discussed in the following subsection.

B. Future Customizable Flyers

With alterations to this test system FWMAV, particularly in the body and transmission structure, we hope to create a flight worthy vehicle while retaining the capability of interchangeable parts. This could lead to unique customizable FWMAVs that are also easy to repair after crashes. When the wings are smaller, they require less power (at similar flapping frequencies). Assuming that the FWMAV is light enough that these wings produce sufficient thrust for flight, then with this system the user has a choice. If faced with a situation where longer flight times are desired but no payload is needed, the user can put on the smaller wings with their corresponding four-bar elements. In situations where a payload is desired but shorter flight times are acceptable then the user can put on the larger wings which produce more thrust and thus support greater weight.

To move in the direction of a freely operating flyer, we acquired a few different lithium polymer batteries in the 0.4-

0.6 g range (FullRiver). To provide a constant voltage to the motor from a single lithium polymer cell, which varies from approximately 4.2 V to 3.3 V during discharge, a lightweight DC-DC boost converter has been designed. The converter is built around the Micrel MIC2296 boost converter IC and implemented on a custom flexible printed circuit board. The output voltage can be adjusted from 4.2 V to 10 V using a trimmer resistor to allow experiments with different supply voltages. The converter has a mass of 200 mg and a footprint of 8 mm by 11mm. Based on motor tests using a benchtop supply, the converter is designed to deliver up to 0.4 A at 6.5 V with an efficiency in the range of 80-88%.

The performance of the flyer using one of these batteries (rather than the power source typically used during the system integration studies) and the boost converter was also recorded on the test stand. The results for the two sized wings are shown in Fig. 9. For these tests, the boost converter was set to deliver 5.5 V. Keeping the rest of the system constant (same motor and four-bar transmission with 0.508mm-thick rubber elements), we compare times that the power delivery remains more or less constant. For the small wing, we are able to run for around 300 s while, for the larger wing, we are able to run for around 100 s. Based on current measurements, the battery is discharged at 9.3C for the smaller wing and at 10.7C for the larger wing. Since the capacity of the lithium polymer batteries decreases with discharge current, for this particular test, this corresponds to an effective capacity of 23 mAh for the smaller wing and 9 mAh for the larger wing, as compared to a 1C capacity of 30 mAh.

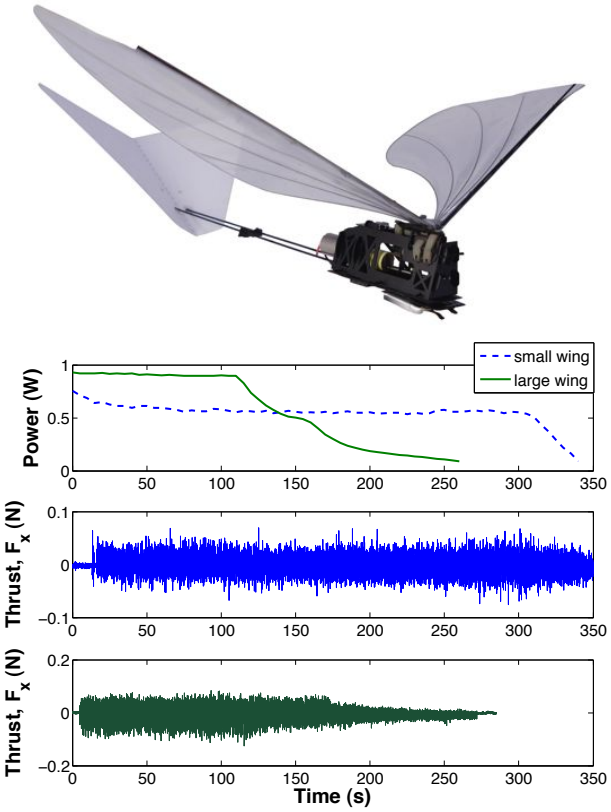

Fig. 9. On the top, a first attempt at an autonomous customizable flyer is shown. On the bottom, results of running the system with a lithium polymer battery and a DC-DC boost converter are shown for both the small and large wing.

V. CONCLUSIONS

An integrated FWMAV platform with interchangeable parts is detailed and its potential for multiple system integration studies regarding wing and transmission configurations is demonstrated. Future studies will involve exploring appropriate spring stiffness and rotation angles for passive rotation in the wing hinge as well as the development of customizable FWMAVs that will allow, through the interchange of parts, a user to customize the system for an intended flight operation.

ACKNOWLEDGMENT

The authors would like to thank Pratheev Sreetharan, Ben Finio, Michael Smith, Mirko Kovac, Jamie Paik, Hiroto Tanaka, Mike Tolley, Andrew Baisch, Katie Hoffman, Kevin Ma, Zhi Ern Teoh, and Vireshwar Sahai for useful discussions and assistance.

REFERENCES

[1] R. S. Fearing, K. H. Chiang, M. Dickinson, D. L. Pick, M. Sitti, and J. Yan, "Wing transmission for a micromechanical flying insect," in *IEEE International Conference on Robotics and Automation*, April 2000.

[2] N. O. Perez-Arancibia, K. Y. Ma, K. C. Galloway, J. D. Greenberg, and R. J. Wood, "First controlled vertical flight of a biologically inspired microrobot," *Bioinspiration and Biomimetics*, vol. 6, p. 036009, 2011.

[3] M. Keennon, K. Klingebiel, H. Won, and A. Andriukov, "Development of the nano hummingbird: A tailless flapping wing micro air vehicle," in *50th AIAA Aerospace Sciences Meeting*. AIAA, January 2012, pp. 2012–0588.

[4] R. J. Wood, "Design, fabrication, and analysis of a 3dof, 3cm flapping-wing mav," in *IEEE/RSJ International Conference on Intelligent Robots and Systems*, San Diego, CA, 2007.

[5] G. C. H. E. de Croon, K. M. E. de Clerq, R. Ruijsink, B. Remes, and C. de Wagter, "Design, aerodynamics, and vision-based control of the delfly," *International Journal of Micro Air Vehicles*, vol. 1, pp. 71–97, 2009.

[6] H. Tanaka, J. P. Whitney, and R. J. Wood, "Effect of flexural and torsional wing flexibility on lift generation in hoverfly flight," *Integravtive and Comparative Biology*, vol. 51, pp. 142–150, May 2011.

[7] T. Pornsin-Sirirak, Y. Tai, H. Nassef, and C. Ho, "Titanium-alloy mems wing technology for a micro aerial vehicle application," *Journal of Sensors and Actuators A: Physical*, vol. 89, pp. 95–103, 2001.

[8] Y. Kawamura, S. Souda, S. Nishimotor, and C. Ellington, *Biomechanisms of Swimming and Flying: Fluid Dyamanics, Biomimetic Robot, and Sports Science*. Springer, 2008, ch. Clapping-wing Micro Air Vehicle of Insect Size, pp. 319–330.

[9] R. Madangopal, Z. A. Khan, and S. K. Agrawal, "Biologically inspired design of small flapping wing air vehicles using four-bar mechanisms and quasi-steady aerodynamics," *ASME Journal of Mechanical Design*, vol. 127, pp. 809–816, July 2005.

[10] H. Takahashi, Y. Aoyama, K. Ohsawa, H. Tanaka, E. Iwase, K. Matsumoto, and I. Shimoyama, "Differntial pressure measurement using a free-flying insect-like ornithopter with an mems sensor," *Bioinspiration and Biomimetics*, vol. 5, p. 036005(7pp), 2010.

[11] W. Bejgerowski, A. Ananthanarayanam, D. Mueller, and S. K. Gupta, "Integrated product and process design for a flapping wing drive-mechanism," *ASME Journal of Mechanical Design*, vol. 131, p. 061006, 2009.

[12] R. Sahai, K. C. Galloway, and R. J. Wood, "Elastic element integration for improved flapping-wing micro air vehicle performance," *IEEE Transactions on Robotics*, p. submitted, 2012.